Cytometry Part A 69A:842–851 (2006)

Single Particle High Resolution Spectral Analysis Flow Cytometry

Gregory Goddard,* John C. Martin, Mark Naivar, Peter M. Goodwin, Steven W. Graves, Robb Habbersett, John P. Nolan,† and James H. Jett

National Flow Cytometry Resource, Bioscience Division, Los Alamos National Laboratory, Los Alamos, New Mexico

Received 15 September 2005; Revision Received 22 April 2006; Accepted 8 May 2006

Background: While conventional multiparameter flow cytometers have proven highly successful, there are several types of analytical measurements that would benefit from a more comprehensive and flexible approach to spectral analysis including, but certainly not limited to spectral deconvolution of overlapping emission spectra, fluorescence resonance energy transfer measurements, metachromic dye analysis, free versus bound dye resolution, and Raman spectroscopy.

Methods: Our system utilizes a diffraction grating to disperse the collected fluorescence and side-scattered light from cells or microspheres passing through the interrogation region over a rectangular charge-coupled-device image sensor. The flow cell and collection optics are taken from a conventional flow cytometer with minimal modifications to assure modularity of the system.

Results: Calibration of the prototype spectral analysis flow cytometer included wavelength characterization and calibration of the dispersive optics. Benchmarking of the system demonstrated a single particle/cell intensity sensitivity of 2160 MESF of R-Phycoerythrin. Single particle spectra taken with our instrument were validated against bulk solution fluorimeter and conventional flow cytometer measurements. Coefficients of variation of integrated spectral fluorescence intensity of several sets of standard fluorescent microspheres ranged from 1.4 to 4.8% on the spectral system. Spectral discrimination of free versus PI bound to cells is also demonstrated.

Conclusions: It is demonstrated that the flow spectrometer has sufficient sensitivity and wavelength resolution to detect single cells and microspheres, including multifluorophore labeled microspheres. The capability to use both standard mathematical deconvolution techniques for data analysis, coupled with the feasibility of integration with existing flow cytometers, will improve the accuracy and precision of ratiometric measurements, enable the analysis of more discrete emission bands within a given wavelength range, and allow more precise resolution of the relative contribution of individual fluorophores in multiply-tagged samples, thereby enabling a range of new applications involving the spectral analysis of single cells and particles. © 2006 International Society for Analytical Cytology

Key terms: fluorescence; spectral analysis; flow cytometry; charge-coupled device; spectral deconvolution; multiplex microsphere analysis

The increasing need for polychromatic approaches to flow cytometry, coupled with rapid technological advances, have driven the design and implementation of instruments that measure up to 19 parameters including 17 fluorescence and 2 light-scatter parameters using multiple lasers for excitation (1). This form of spectroscopy is almost universally employed in flow cytometers. In many commercial cytometers, the wavelength bands that each detector responds to are fixed. In others, the wavelength bands are adjusted by changing beam splitter-filter combinations as experiments require.

However, the need to simultaneously detect even greater numbers of fluorescence signals may soon outstrip the abilities of even these systems. One solution is to increase the number of detectors using even narrower bandpass filters (2–5). An alternate solution would be a shift of paradigm from capturing discrete wavelength subsets via filter separation to acquisition of higher resolution spectra using wavelength dispersive optics.

Several approaches to higher spectral resolution using dispersive optics in flow have been reported. They fall primarily into four categories: wavelength scanning, interfer-

Grant sponsor: National Flow Cytometry Resource (NIH); Grant number: RR-01315.

†Present address of John P. Nolan: La Jolla Bioengineering Institute, 505 Coast Boulevard South Suite No. 405, La Jolla, CA 92037.

*Correspondence to: Gregory Goddard, National Flow Cytometry Resource, Bioscience Division, MS M888, Los Alamos National Laboratory, Los Alamos, NM 87545.

E-mail: ggoddard@lanl.gov

Published online in Wiley InterScience (www. interscience.wiley.com).

DOI: 10.1002/cyto.a.20320

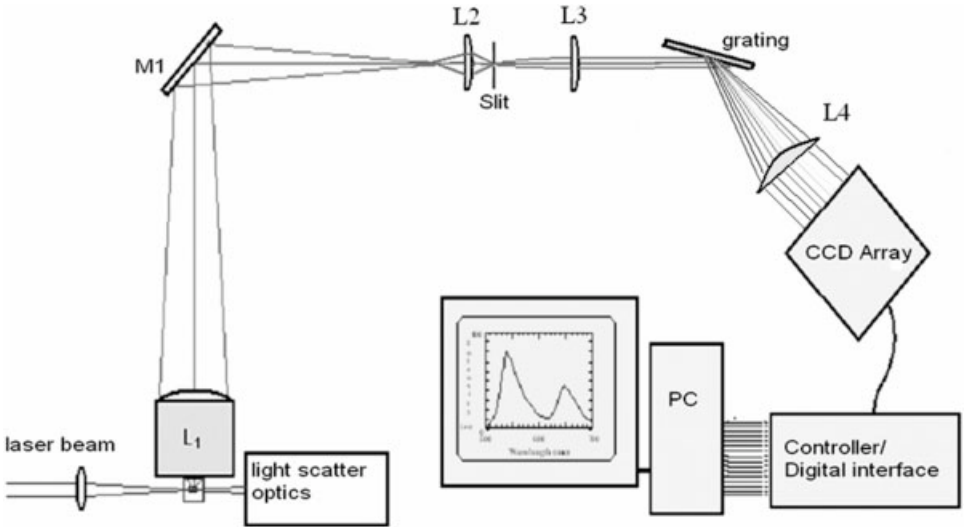

FIG. 1. Schematic of spectral flow cytometer experimental apparatus with grating dispersive element. L1 is a $f = 150$ mm BD collection lens system gel-coupled to the flow cell. L2 is a $f = 10$ mm refocusing lens. L3 and L4 are the collimation lenses inside the Kaiser grating spectrograph. The Hamamatsu CCD array is interfaced to a National Instruments data acquisition card in a PC. [Color figure can be viewed in the online issue, which is available at www.interscience.wiley.com.]

ogram encoding, multispectral imaging, and grating or prism dispersion onto array detectors.

Howard et al. (6) described the use of a wavelength scanning monochromator attached to a flow cytometer as a fluorescence detector. A similar approach was reported by Stokke and Steen (7,8). Measurement of complete single-particle spectra by a flow cytometer was reported by Buican et al. (9). His approach was to couple a Fourier-transform spectrometer to the cytometer, thereby encoding the spectral information in an interferogram.

Isailovic et al. (10) investigated a fluorescence spectrometer with one dimensional imaging, capable of single cell analysis in flow based on a system developed by Ma et al. (11), whereby the light captured from the flow cell was dispersed, via a grating, onto an intensified charge-coupled device (CCD) array in one dimension. In a separate development to achieve spectral imaging in flow, Amnis (Seattle, WA) uses conventional filters to disperse the light into several distinct image sensor regions while synchronizing CCD readout to particle passage through the flow cytometer probe volume (12–15).

Another approach is to disperse the collected light and use a linear, position encoded detector to record fluorescence intensity as a function of wavelength. The earliest implementation of spectral analysis capability in flow cytometry utilized dispersive optical elements coupled to vidicon image sensors (16–18). Some of the inherent photosensitivity issues for these sensors have been bypassed with the introduction of solid state array detectors. Three groups have reported using solid-state array detector technology in flow cytometry. Using a photodiode array behind a gated multichannel plate intensifier and a prism spectrograph coupled to a flow cytometer, Gauci et al. (19) detected the fluorescence spectra of muliple fluorophore-stained cells and highly fluorescent microspheres. Robinson et al. (20,21) reported the use of a multi-anode photomultiplier coupled to a flow cytometer with a dispersive grating to acquire spectral information from cells in flow. Fuller and Sweedler coupled a grating spectrograph to a flow cytometer (21) to individually identify, size, and discriminate microspheres based on fluorescence intensity and spectral peak position. Dubelaar et al. incorporated a holographic grating and multipixel hybrid photodiode into their buoy flow cytometer to autonomously gather data on phytoplankton for environmental monitoring applications (22).

Our system, which also utilizes a CCD image sensor coupled to a spectrograph, is designed for optimal modularity. The system is built around the flow cell and collection optics of a conventional flow cytometer with minimal modifications. This has been accomplished using a volume-phase holographic transmission grating in an imaging spectrograph to disperse the collected fluorescence emitted by cells or microspheres as they pass through the interrogation region within the flow cell. The experimental setup is described, followed by a presentation of the intensity and spectral sensitivity evaluation. Several of the unique benefits of higher spectral resolution to flow cytometry are also demonstrated.

MATERIALS AND METHODS

Instrument

The system is constructed around a BD FACSCalibur optical platform (Becton Dickinson Immunocytometry Systems, San Jose, CA) flow chamber and fluorescence/light scatter collection optics (Fig. 1). Crossed cylindrical lenses are used to focus the laser beam to an ellipse ~290 μm wide by 50 μm high. The collection optics have a back focal length of ~150 mm. An adjustable lens with a focal length of 10 mm is placed about 1 cm beyond that focal point to refocus the collected light onto the fixed 200 μm slit prior to recollimation within a Holospec HS-f/2.2-Vis spectrograph (Kaiser Optical Systems, Ann Arbor, MI) spectrograph with a model 2004372-502 HVG-590 linear dispersive grating. The grating disperses the light over the face of a thermo-electrically cooled back-thinned 1024 × 128 pixel Hamamatsu (Hamamatsu Photonics, Sunayama-

cho, Japan) CCD array with spectral separation along the long axis of the array. The pixels were ~24 μm^2. The light is incident on ~75% of the height of the CCD to assure efficient light collection. The columns of the CCD chip are summed vertically on-chip to increase effective pixel size, and thereby collection efficiency. The CCD array is interfaced to a AT-AI-16XE-10 National Instruments (Austin, TX) data acquisition board controlled by a LabView (National Instruments) data acquisition program provided by Hamamatsu. This CCD array was chosen due to the inherent quantum efficiency of a back-thinned CCD, which exceeds 80% for the wavelength region of 500–800 nm with peak sensitivity of ~92% as reported on the manufacturer-supplied datasheet. To reduce scattered laser light intensity on the CCD, a 515 dichroic longpass filter was used between the collection optics and the dispersive optics. It is a standard DL filter giving a plateau longer wavelength transmission of 90–99% (data not shown) while blocking of typically 99.9% of the shorter wavelength with a relatively shallow slope (~5–10 nm ramp to the plateau) at the listed wavelength.

In preliminary experiments, a prism was used in place of the spectrograph (23). The nonlinear dispersion of a prism allows for higher spectral resolution of either shorter or longer wavelengths, depending on angle of incidence of the dispersed light onto the array and does not lose light to higher order diffraction. Although a prism provides potentially higher fluorescence detection sensitivity measurements, the grating spectrograph used was chosen for the experiments reported here because of its nearly linear dispersion over the wavelength range and array dimensions used and the ease of modular integration with existing flow cytometers.

Excitation

An argon ion laser and a mercury arc lamp were used for these experiments. The argon-ion laser was a 5 W Innova 90 laser from Coherent (Santa Clara, CA) and the mercury lamp used for illumination was a 100 W Carl Zeiss (Thornwood, NY) stabilized arc lamp. Calibration of other spectral systems has included the use of mercury lamps (24) and fluorophores (19). Several approaches can be taken, in practice, for spectral calibration. Atomic emission lamps are available from a variety of manufacturers containing single gases, such as H, He, Ne, Ar, Kr, and Xe, metal vapors such as Hg, Tl, Na, and Zn, and combinations thereof, such as Hg–Ar and Hg–Cd. Such lamps have discrete emission lines ranging from 200 nm out to over 900 nm. Alternatively, several NIST-certified spectral irradiance lamps such as tungsten–quartz halogen and high pressure metal vapor are available with continuous broadband blackbody irradiance spectra over a range from 200 to 1400 nm (25). As another alternative, lasers can be used as spectral calibration sources for both spectral line width and wavelength due to the extreme monochromaticity of laser emission. More thorough review of spectral calibration techniques can be found elsewhere (25–30). This system was wavelength-calibrated against scattered laser light at five argon ion laser wavelengths, 465 nm, 476.5 nm, 488.0 nm, 496.5 nm, and 514.5 nm. Points corresponding to Raman scatter of each of the laser lines off water were also used for calibration. The argon laser lines are known to be extremely spectrally narrow and the peak positions and shapes of Raman scatter off water are well known (31). Additional lines from the arc lamp, at 404.7, 435.8, 546.1, and 580.0 nm, were also used for the wavelength calibration, also through scatter off of beads. The benefit of using laser scatter in addition to arclamp scatter is the accuracy of colocalization of the illumination and light collection foci. The laser and Raman signals are equivalent to those expected during normal flow cytometry operation as the optical interrogation region is identical. The arclamp was focused to the center of the flow cell and also scattered off of blank polystyrene microspheres to attempt to match the same conditions. Arclamp illumination is more problematic as small misalignments of the illumination focus will result in variations in the angle of incidence on the grating or prism, and consequent errors in spectral calibration. The fourteen wavelength points used for spectral calibration were chosen based on availability; future instruments could be calibrated using more even sampling of wavelength space, thereby generating a better regression fit to either polynomial or transcendental functions.

With the exception of the wavelength calibration measurements, all samples were analyzed at ~100 mW using the 488.0 nm laser wavelength. Because of the well-known dispersion relations of gratings, interpolation and extrapolation based on a polynomial fit to the calibration wavelength versus pixel number data is possible. Because of our larger stream diameter, arising from the slower flow rates, a larger elliptical spot size (290 × 50 μm^2) than the FACSCalibur (66 × 20 μm^2) was used. At these spot sizes and the corresponding excitation powers used, the average optical power density in our system is roughly 8.4 $\mu W/\mu m^2$ in the spectral system compared to the 14.4 $\mu W/\mu m^2$ used in the FACSCalibur. Factoring in the particle transit times through the excitation laser beam in each instrument, the optical exposure energies are 0.053 and 0.055 $nJ/\mu m^2$ for the Spectral and FACsCalibur, respectively. So although 100 mW of laser power was used for these experiments, lower excitation power would be expected to work equally well under similar optical excitation conditions.

Sample Delivery

All samples were delivered at 15 μl/min using a Yale Apparatus (Wantagh, NY) Multiphaser model YA-12 syringe pump. For wavelength calibration measurements, the concentration of particles was ~1 × 10^6 particles/ml; for all other measurements, the particle concentration was ~1.7 × 10^5 particles/ml to minimize coincident events during the exposure and readout intervals of the CCD array. The sheath was run at a flow rate of 3 ml/min, yielding a particle transit time of about 14 μs and a sample core diameter of ~15 μm. For all measurements except wavelength calibration, the sample analysis rate was about 42 particles per second. While relatively low concentrations were

Table 1
Microspheres Used for Wavelength Calibration and Sensitivity Analysis

No.	Microsphere	Fluorophore	Diameter (μm)	Spectral CV (%)	FACS CV (%)	Supplier
1	Polymicrospheres	*None*	10	–	–	Polysciences[a]
2	YG polymicrospheres	Fluorescein	1.8	4.5	2.5	Polysciences
3	PC-Red	Phycoerythrin	2	1.4	2.3	Polysciences
4	Fluorospheres	Nile Red	2	11	2.8	FCSC[b]
5	Fluorospheres	Tetramethylrhodamine	9	4.8	2.4	FCSC
6	Blank (0 MESF)	R-Phycoerythrin	7.4	–	–	FCSC
7	1648 MESF	R-Phycoerythrin	7.4	11	2.1	FCSC
8	4784 MESF	R-Phycoerythrin	7.4	10	2.2	FCSC
9	23777 MESF	R-Phycoerythrin	7.4	8	2.0	FCSC
10	61908 MESF	R-Phycoerythrin	7.4	8	1.8	FCSC
11	Biotin-coated	Strepavidin-coated quantum dots	6.4	6.2–8.5	4.8	Spherotech[c]

Fluorescence coefficients of variation (Fl CV) measured on FACs Calibur flow cytometer for each sample with 488 nm excitation corresponded well to manufacturer reported values. Spectral CVs measured on spectral flow cytometer for each sample at 488 nm excitation.
[a]Polysciences (Warrington, PA).
[b]FCSC (now available from Invitrogen, Carlsbad, CA).
[c]Spherotech (Libertyville, IL).

used for these experiments, faster CCD readout electronics would allow higher analysis rates without coincidence.

Bead Samples

For each of the microsphere samples, a background "spectrum" was recorded using a DI water sample at an identical volumetric delivery rate with manual triggering with an identical exposure time. The background spectrum is subtracted, when indicated, from the sample spectra to remove flow cell scattered laser light and Raman scatter from the water. A similar technique can be used to remove background fluorescence from free fluorophores or average autofluorescence of cells.

Several types of microspheres were used for calibration, sensitivity determination, and validation as listed in Table 1. The first microsphere type listed was used for calibration of the system based on scatter of laser light at specific wavelengths. The next four microsphere types listed were used for verification of spectral calibration. The next five microsphere types listed were used to verify intensity linearity and determine limits of sensitivity. The last microsphere type listed was used as a substrate for binding Strepavidin-coated quantum dots (QD) from Q-dot Corporation (Hayward, CA) with emission wavelengths of 565, 605, and 655 nm. These QD-tagged microspheres were used to verify spectral discrimination of closely-spaced fluorophores as well as wavelength calibration. Microsphere samples were suspended in DI water, and hydrodynamically focused using DI water as sheath fluid.

Cell Sample

A demonstration of free fluorophore background subtraction was performed with propidium iodide-stained human promyelocytic leukemia (HL-60) cells. They were grown and harvested following the procedure described in Cui et al. (32). The cells were fixed in 70% ethanol, resuspended in PBS, and stained with PI at a concentration of 5 μg/ml. The sheath fluid was also PBS buffered for cell measurements.

Verification Measurements

Additional experiments to verify the accuracy of fluorescence CV measurements were carried out by running selected samples on a BD FACSCalibur. Triggering was performed on forward scatter with acquisition of side scatter and three channels of fluorescence with 488 nm laser excitation. The filter set was a 530/30 filter on fluorescence channel 1, a 585/42 filter on fluorescence channel 2, a 661/16 filter on fluorescence channel 3. Voltage settings on each of the PMTs were set for each sample to take advantage of the dynamic range of the instrument. The sample was run at 60 μl/min. Spectrofluorimeter data presented was taken on a Photon Technology (Birmingham, NJ) spectrofluorimeter with dual monochromator arc lamp excitation and dual emission measurements using photon-counting PMTs. The arc lamp was operated at 75 W, with entrance and exit slit widths optimized for signal transmission with minimal wavelength crossover on each monochromator. The PMTs were operated at 1000 V.

Triggering

Each of the spectral measurements was taken on single microspheres or single cells, to demonstrate single particle sensitivity. Several spectra are shown for each type of particle or cell to demonstrate reproducibility. Several triggering mechanisms were used, including a "one-shot" circuit that outputs a 5 V logic pulse on side-scattered laser light above a threshold, software triggering on a threshold of integrated intensity on the CCD, and via a single channel analyzer/counter of side-scattered light.

Single Particle Detection

Single particle detection was assured through an acquisition trigger threshold and postacquisition analysis. The acquisition trigger threshold was set above background-scattered light to assure detection of particle passage and rejection of spurious side-scatter PMT noise. This assured that recorded spectra contained at least one particle. Coincidence rejection was performed by selecting only spectra

containing the lowest multiple of scatter and fluorescence peak values after background subtraction. Further verification of noncoincidence was achieved by monitoring the signal directly out of the side-scatter PMT on a Tektronix (Beaverton, OR) digital oscilloscope synchronized to the shutter exposure signal of the CCD camera.

Data Analysis

The CCD data were saved in XLS file format and subsequently exported into Excel (Microsoft, Redmond, WA). Background subtraction was performed on a column-by-column basis. Standard deviations were calculated on integrated peak fluorescence values from several spectra of individual particles. Coefficients of variation of integrated peak fluorescence were calculated as the SD over the mean value for each particle multiplied by 100 to express as a percent. The lower limit of detection for MESF microspheres is determined as the *X*-intercept of the upper limit of the error bar of the blank microspheres. After statistical analysis, the data was then exported into SigmaPlot (Systat Software, Point Richmond, CA) for graphical display.

RESULTS

Spectral Calibration

The system was calibrated by running a sample of 10 μm nonfluorescent polystyrene microspheres from Polysciences (Table 1) diluted to a concentration of ~1 × 10^6 particles/ml. The laser output was then successively tuned to 457.9, 476.5, 488.0, 496.5, and 514.5 nm emission lines. Several example spectra of scattered laser light dispersed across the CCD are shown in Figure 2A. The narrow peaks at lower pixel numbers (shorter wavelengths) correspond to the Rayleigh-scattered laser light, while the broader, longer wavelength peaks correspond to Raman scatter from the stretching mode of water. The pixel position of the dispersed scattered laser light (solid circles), Raman scatter from the stretching mode of water (solid triangles), and dominant mercury lines (open circles) are plotted against expected wavelength in Figure 2B. A linear regression analysis yields an R^2 factor of 0.9998. When the same data is fit with a sinusoid, and the predicted pixel to wavelength conversion is extrapolated up to 800 nm, the deviation from a linear fit is about 0.13%. This equates to ~1 nm, which is also the spatial resolution of our CCD array. A two sigma confidence interval of the regression line is ~0.2% or 1.79 nm, based on the standard error of estimate at 800 nm. If we expand to a second order (quadratic) fit, the R^2 goes to 0.99999 with an extrapolated deviation from the cosine of about 0.012% at 800 nm. Since that corresponds to a deviation of ~0.08 nm and our spatial, and thereby wavelength resolution, is only 1 nm, any higher order polynomial regression equations would overlay the linear fit and therefore be indistinguishable from that line by virtue of the pixel size on the CCD. The equation for the line was used to transform pixel number to wavelength and plot the data shown in Figures 4–6.

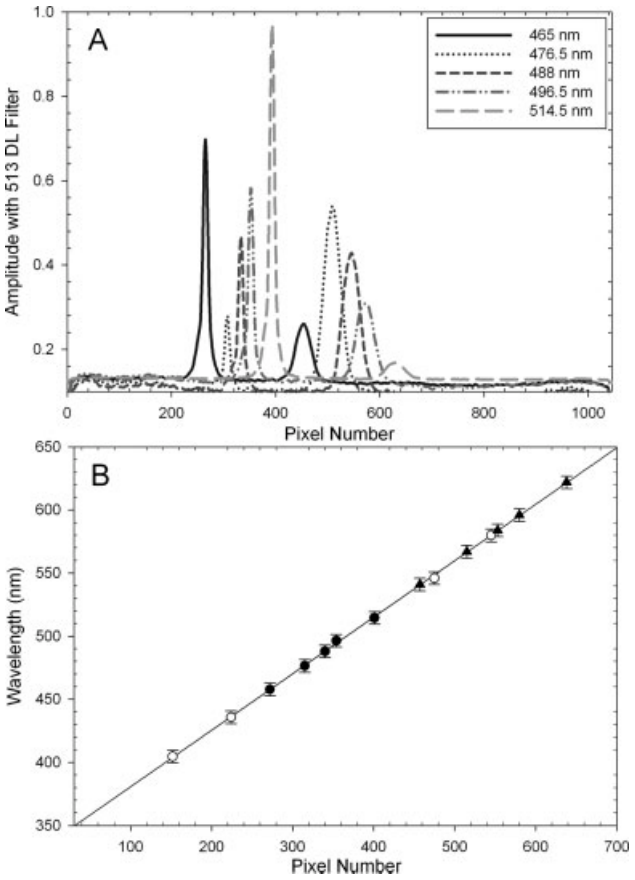

FIG. 2. (**A**) Example of spectra from laser light scatter and Raman scatter from the stretching mode of water, taken with a 515 DL filter. (**B**) Graph of laser light scatter (solid circles), Raman scatter from the stretching mode of water (solid triangles), and mercury arc lamp scatter (open circles) wavelengths against pixel position after dispersion. Linear fit included all data shown with the R2 value greater than 0.999. Error bars indicate one SD of repeated measurements. [Color figure can be viewed in the online issue, which is available at www.interscience.wiley.com.]

Intensity Linearity and Sensitivity Determination

The next set of experiments was used to determine the limits of sensitivity and verify the linearity of intensity measurements. Five sets of R-phycoerythrin (R-PE) MESF microspheres (Table 1) were used for the experiments at levels from 0 to 61908 molecules of R-PE (34). Figure 3 represents the integrated spectral peak area values against the MESF value of the microspheres. A background signal, taken with a DI water sample, was subtracted from the spectral data prior to representation and analysis. Standard deviations of the integrated fluorescence intensity for each particle were determined based on ~100 single particle spectra for each of the microsphere sets. The error bars indicate two standard deviations above and below each point for each of the microsphere sets (98% confidence level). A linear fit of the spectral data (ignoring the blank) has an R^2 value of 0.9724 and a resultant lower limit of detection of 2161 R-PE molecules was determined using the method of Gaigalas et al. (34). Using the same method, our FACsCalibur demonstrated a sensitivity of ~498 MESF

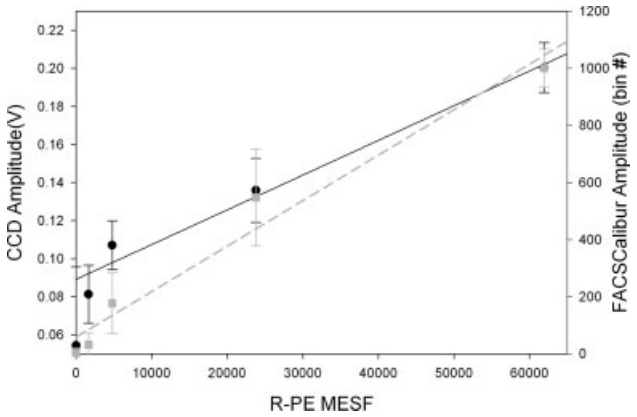

FIG. 3. Graph of detector response against R-PE MESF microsphere fluorescence excited at 488 nm. Linear regression fit does not include blank bead. Error bars above and below each point indicate two SDs of successive single bead spectra. Each data point is the integrated area under the fluorescence peak. The linear regression of the spectral data (black) has an R2 value greater than 0.972 and corresponds to ~100 single particle spectra per point. A background signal from DI water has been subtracted before representation of the spectral data. The linear regression of the FACSCalibur data (gray) has an R2 value greater than 0.98 and corresponds to ~5,000 single particle spectra.

PE. In comparison, a conventional FACSCalibur has a sensitivity of 300–500 fluorescein molecules, which are roughly 7 times dimmer than PE molecules, when well aligned (35–37). The limits of intensity sensitivity of our spectral instrument are due to electronic noise and losses within the collection optics. The electronic noise consists of dark current, readout noise, and digitization noise.

System Validation

Several different types of fluorophore-impregnated polystyrene microspheres were used to verify the stability of the spectral measurements. The particle size and fluorophore type for each is summarized in Table 1. The results are represented graphically in Figure 4. A background signal, taken of DI water, was subtracted from each spectrum. As can be seen for each type of microsphere, the intensities of the fluorescence spectra exhibit a fairly narrow intensity distribution. The calculated coefficient of variation (CV) of integrated peak fluorescence for the R-PE microspheres was ~1.4%. The YG Polymicrospheres Tetramethylrhodamine microspheres integrated peak fluorescence CVs were 4.5 and 4.8%, respectively. The Nile Red Polymicrospheres CV was 11%. Reference CVs, measured on a conventional flow cytometer, were 2.3–2.8% (data not shown).

To further validate the system, as well as verify spectral discrimination capabilities, the emission spectra of three populations of strepavidin-coated quantum dots (QD), separately and collectively attached to biotin microspheres, were measured in the spectral system and compared to fluorimeter measurements. There were $\sim 1 \times 10^5$ quantum dots per microsphere in each case. The results of this experiment are graphically represented in Figure 5. Comparison of the bulk fluorimeter spectra in Figure 5A to the spectral flow cytometer data in Figure 5B shows good correlation. The choice of 565, 605, and 655 nm quantum dots was based on their availability and relative fluorescence intensities. Each line color corresponds to a population of microspheres with a particular QD attached. A fourth set of microspheres was tagged with equimolar quantities of each QD. Each of the constituent quantum dot spectra can be seen on the multiple QD-tagged microspheres. The calculated coefficients of variation for the 565, 605, and 655 nm individual wavelength QD-tagged microspheres were 8.5, 7.3, and 6.2%, respectively. This is expected if variable relative numbers of each type of quantum dot is attached to each microsphere. Further investigations will use more uniformly-tagged microspheres with monodisperse QDs. Other probable explanations for the higher CVs measured by the spectral flow cytometer, as compared to the conventional flow cytometer (Table 1), are the broader sample stream diameter and consequent variation in excitation by the laser and the relative proximity of the fluorescence intensities to the noise floor of the CCD. It can be seen in the graph that there is distinct and

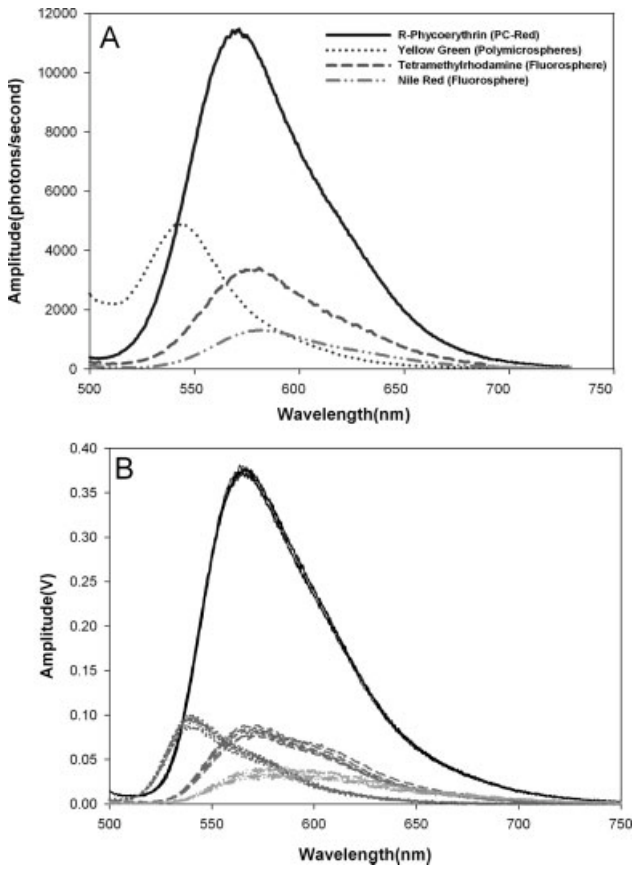

FIG. 4. Graph of fluorescence spectra from four different microsphere fluorophores (Table 1), excited at 488 nm. Each line type corresponds to a population of microspheres tagged with a particular fluorophore. (**A**) Spectra from ensemble average of the population of microspheres measured with a PTI fluorimeter at the same bead concentration as for spectral flow measurements. (**B**) Ten individual spectra from single microspheres measured with the spectral flow cytometer; A background signal from DI water has been subtracted from each single-bead spectrum.

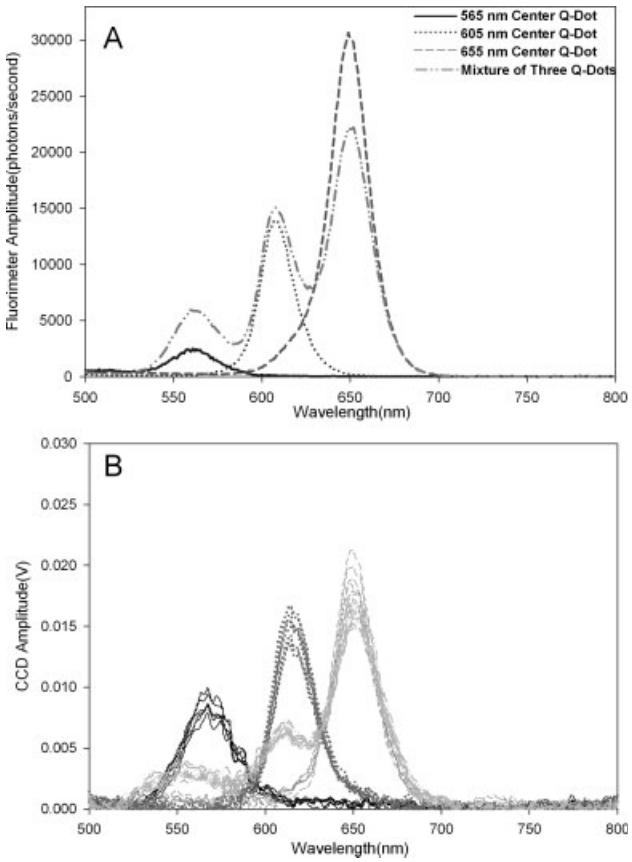

FIG. 5. Graph of fluorescence spectra from biotin microspheres labeled with three different types of strepavidin-coated quantum dots with 488 nm, 100 mW excitation. Each quantum dot had a center fluorescence at the specified wavelength. (**A**) Spectra from samples of quantum dot-labeled microspheres measured with a PTI fluorimeter. (**B**) Ten individual spectra from single microspheres measured with the spectral flow cytometer; A background spectra from DI water has been subtracted from each singlebead spectrum.

reproducible separation of the three QD components in the fluorescence spectra. Gao and Nie showed that by "staining" microspheres with various combinations of quantum dots, it is possible to take advantage of both wavelength- and intensity-encoded microspheres for multiplex assays (38). While they achieved 11 different QD-encoded microsphere populations with conventional flow cytometry, the greater spectral resolution of our instrument would allow for even greater numbers of unique encoding combinations of quantum dots.

Cell Measurements

For a preliminary demonstration of the applicability to a biological system, as well as the removal of background contributions, HL-60 cells were fixed in ethanol and stained with 5 μg/ml PI. Spectra of PI in the sample stream and individually PI-stained cells were captured for comparison. The data are shown in Figure 6. A water background spectrum and a PI background spectrum were recorded for comparison with spectra from individual PI-stained cells under identical flow conditions. The water "background" spectrum was subtracted from the PI spectrum on each of the cells analyzed. As visible in the graph, when comparing the magenta and red traces, which include background contributions, with the blue traces, where the PI "background" has been subtracted, the contribution of Raman scatter from water can be removed. The relative narrow intensity distribution corresponded to all cells being in the plateau phase, as we confirmed with conventional flow cytometry (data not shown). The green trace at the bottom of the figure corresponds to the free PI in solution after the water background was subtracted. Since background and sample spectra were captured and saved separately, no information was lost. This spectral subtraction also demonstrates the ability to remove background signals such as Rayleigh or Raman light scatter, and/or cell autofluorescence.

DISCUSSION

The goal of this work was to develop a modular technique for incorporating continuous spectral analysis of single particles and cells from 400 to 800 nm in a flow cytometer. To minimize cost and complexity, we used wavelength dispersive optics and an array detector to capture the complete spectra. The use of dispersive optics creates a simpler optical system, while potentially reducing the instrument cost through the elimination of precision wavelength filters. The simpler optical train helps reduce light losses within the system, thereby contributing to greater measurement sensitivity. The optical design of this

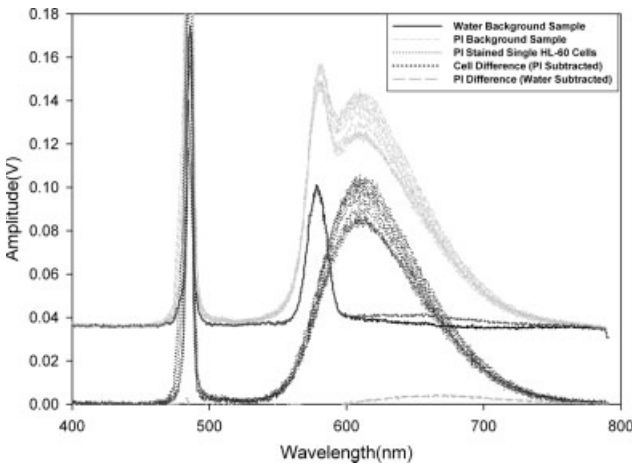

FIG. 6. Spectra of fifteen individual PI-stained HL-60 cells excited with a 488 nm laser. The black line corresponds to the background spectra with only water in the sample stream. The dotted line indicates the background spectrum of PI in the sample stream in the absence of cells, the light gray short dashed lines correspond to individual PI-stained cells, and the dark gray dashed lines are the difference of each cell spectrum and the PI background. The light gray line is the difference of PI-only sample from the water background. The leftmost peak is the scattered laser light, the narrow peak near the center, most visible in the two background spectra, corresponds to the Raman scatter due to the stretching mode of water, and the broad peak corresponds to PI fluorescence. The rightmost peak in the background-subtracted PI-only spectrum corresponds to unbound PI, while the narrower and higher peak visible in the background-subtracted sample spectra corresponds to bound PI.

system would allow for retrofit of nearly any conventional flow cytometer. Separately, the use of a CCD array detector removes the need for separate PMTs and associated high voltage power supplies. The selection of a back-thinned CCD versus a front-illuminated CCD and use of summing of array rows, provides greater photon collection and photoelectron conversion efficiency, and thereby increases the signal to noise ratio. Toward the goal of modularity, a relatively low noise commercial data acquisition card is used for control, readout, and signal digitization. The elimination of dependence on filters also allows greater experimental flexibility.

In benchmarking the spectral flow cytometer, larger coefficients of variation were observed for spectral data as compared to conventional flow cytometer data. A probable explanation for this effect is the proximity in signal amplitude to CCD readout and dark current noise. In this signal range, the influence of background fluctuations is greater. Although readout noise is introduced by horizontal and vertical shift registers as well as the ADC, the ADC noise is the larger contributor. The full digitization range extends from 0 to 10 V. In comparison, typical signal amplitudes for single particle measurements range from 0.05 to 0.2 V. This equates to ~2% of the dynamic range of the ADC. By performing on- or off-chip summing of the pixels before the data is digitized, much of this digitization noise can be overcome. Alternatively, the gain can be increased on the analog readout signal prior to digitization, thereby taking advantage of a greater proportion of the dynamic range of the ADC. As many ADCs also have the capability of changing their range of digitization voltages, it is also possible to select the digitization range more optimally to sample the signals. Dark current can be further reduced by signal averaging, and by additional cooling of the image sensor. The latter is more appealing than the former, since it maintains a ratio of one particle per spectra. Additional deviation of the data from the mean would also be expected from the increased sample stream diameter arising from the slower flow speed used in the spectral flow cytometer.

While we have shown that this optics and detector configuration would support full spectral analysis capability of single particles on a conventional flow cytometry platform, several challenges remain to make the promise of spectral analysis a reality. Future improvements to the system will include implementation of faster image capture, better triggering, more efficient utilization of ADC dynamic range, and noise reduction circuitry. It is anticipated that such improvements could allow comparable sensitivity to a commercial flow cytometer. To fulfil these requirements and allow for the rapid capture and real-time analysis of the large data sets generated by the spectral flow cytometer, a new digital data acquisition system is under development at the National Flow Cytometry Resource. Integrated into this effort is both acquisition hardware and data analysis software development to support the new spectroscopic applications made possible by the ability to collect full fluorescence spectra from single cells and particles.

The system performance is demonstrated for several different fluorophores, including QD-conjugated microspheres and stained mammalian cells. The potential of using quantum dots to encode addresses in a microsphere array system was also discussed. Preliminary benchmarking of the system demonstrated single particle sensitivity down to 2160 MESF R-PE. It is anticipated that future improvements to the electronics and optics will allow for spectral resolution of even weaker signals. Although sample stream diameters were slightly greater than conventional flow cytometers, fluorescence CVs were observed to be comparable. Comparisons of bulk solution fluorimeter measurements showed good correlation to the single particle spectra taken with our instrument. Furthermore, it was demonstrated that the spectral flow cytometer has sufficient spectral discrimination for detecting multiplex quantum dot-encoded microspheres.

In the validation experiments, YG Polymicrospheres demonstrated a clear red shift in emission wavelength from the standard emission spectra of fluorescein in water. This shift is most likely due to the embedding of the fluorophore in the microspheres and the resulting difference in fluorophore microenvironment. The other fluorophores do not exhibit the same shifts, suggesting that they are less sensitive to their environment. The ability to resolve small shifts in peak fluorescence wavelength due to fluorophore environmental changes suggests intriguing possibilities for greater elucidation of biological systems.

While the focus of this work was the development, calibration, and benchmarking of a modular spectral flow cytometer instrument, it was motivated by several types of analytical measurements that would benefit from a more comprehensive and flexible approach to spectral analysis in flow cytometry. Primarily, higher spectral resolution affords the ability to separate closely-spaced or overlapping fluorophores, background autofluorescence, and light-scatter with greater precision, thereby allowing better component quantitation. In conventional flow cytometry, crosstalk and bleed-through from separate probes is generally addressed by compensation between the spectral channels, while background autofluorescence and/or light scatter leakage are often subtracted from the final population average. Greater numbers of emission bands of interest increases analysis complexity, requires extensive compensation, careful gating, proper filter selection, and experimental design, often including the use of fluorescence minus one (FMO) control samples (1,38–41). A similar problem of deconvolution is faced in spectroscopy, where the entire emission spectrum is collected (42–45). Consequently, several mathematical deconvolution techniques have been developed to separate backgrounds and discrete spectral components (46–48). Some algorithms have even shown success at separating signal components with little or no a priori information about the sample (49,50). In our full spectral flow cytometer, it is possible to take advantage of data analysis techniques from both fields.

By proper summing of array elements to create the appropriate "virtual" filters, it could be possible to use

conventional flow cytometry fluorescence compensation techniques. These "virtual filters" would allow data compression in the form of binning, thus allowing the generation of standard FCS file formats with "programmable bandwidth filters." Moreover, since the entire spectra are stored, no data is lost; new files can be generated with different virtual optical filters applied to the same data set. Once the FCS files are generated, standard flow cytometry data analysis programs can be used for the remaining analyses. Complementary to this analysis, by collecting the entire emission spectra, it becomes possible to use standard mathematical deconvolution techniques, similar to the techniques used in steady-state spectrofluorimetry, to separate backgrounds and closely-spaced fluorophores, while still maintaining quantitative intensity information, as would be required for accurate spectral deconvolution. The data sets could then be analyzed using either multivariate analysis software commonly used by analytical spectroscopists in a batch-processing mode, or the mathematical deconvolution algorithms can be applied prior to export of each fluorophore spectral contribution to a separate bin of an FCS file. Alternatively, the deconvolution algorithms could be used to generate more accurate compensation matrices for standard flow cytometry compensation. While data compression approaches such as these can be used to reduce the total size of the data set needing analysis, the additional information present in the original spectra allows enormous flexibility of data post-processing, even allowing the experimenter to change filters, and mirrors in the system "virtually" after acquisition of the data to gain the information desired.

In several types of applications, probe fluorophores will possess different emission spectra in the free versus bound states or in different environmental conditions, such as calcium concentration, pH, and fluorophore binding state (51,52). Metachromic dyes, such as Acridine Orange, exhibit different emission spectra dependent upon binding mode. In fluorescence resonance energy transfer (FRET), the efficiency of the energy transfer is dependent on the overlap of the donor emission with the acceptor excitation spectra, their dipole orientations, and the proximity of the two fluorophores. While ratiometric measurements are typically used to resolve the environmental conditions, various binding states, or FRET efficiency, higher spectral resolution would allow more accurate wavelength discrimination, thereby enabling better quantification. Furthermore, the ability to apply "virtual" filters of arbitrary wavelength and bandwidth to the resultant spectrum could provide greater flexibility in fluorophore selection.

Finally, in another application that is gaining in importance, emission spectral analysis can be used to decode microsphere array addresses in multiplexed bead-based analyses (53). While the current approaches to encoding microsphere arrays use organic fluorophores with fairly broad emission spectra, such as the Luminex system (Luminex Corporation, Austin, TX), the increasing availability of nanocrystals (quantum dots) with relatively sharp emission spectra makes it feasible to consider detecting several fluorophores within a fairly narrow wavelength range, thereby allowing more complex multiplexing designs. The higher resolution of our instrument makes it possible to spectrally discriminate closely-spaced fluorescence peaks, thereby enabling the use of a larger number of fluorophores, yielding greater versatility of spectral encoding.

In conclusion, the ability to use standard flow cytometric compensation or mathematical spectral deconvolution routines will improve the accuracy and precision of ratiometric measurements, enable the analysis of more discrete emission bands within a given wavelength range, reduce detector crosstalk, and open the door to a range of new applications involving the spectral analysis of single cells and particles. Through the integration of these capabilities, the possibility of an inexpensive, more flexible, and portable flow cytometer could be realized.

ACKNOWLEDGMENTS

The authors would like to express their appreciation to Jim Parson for his invaluable electronics support, and Dr. James Freyer for many helpful discussions. We also acknowledge the advice of Kevin Albright in the early planning phase of this work, and especially for suggesting the use of the back-thinned CCD array. The authors would also like to thank Travis Woods for providing beads and quantum dot samples and Claire Sanders for providing stained HL-60 cells.

LITERATURE CITED

1. Roederer M. Spectral compensation for flow cytometry: Visualization artifacts, limitations, and caveats. Cytometry B Clin Cytometry 2001; 45:194–205.
2. Perfetto SP, Chattopadhyay PK, Roederer M. Innovation—Seventeen-colour flow cytometry: Unravelling the immune system. Nat rev Immunol 2004;4:648–655.
3. Perfetto SP, Roederer M. New advances in flow cytometry: How to do successful polychromatic flow cytometry. Cytometry B Clin Cytometry 2004;59:98–99.
4. Roederer M, Brenchley JM, Betts MR, De Rosa SC. Flow cytometric analysis of vaccine responses: How many colors are enough? Clin Immunol 2004;110:199–205.
5. Roederer M, Treister A, Moore W, Herzenberg LA. Probability binning comparison: A metric for quantitating univariate distribution differences. Cytometry B Clin Cytometry 2001;45:37–55.
6. Asbury CL, Esposito R, Farmer C, vanden Engh G. Fluorescence spectra of DNA dyes measured in a flow cytometer. Cytometry B Clin Cytometry 1996;24:234–242.
7. Steen HB, Stokke T. Fluorescence spectra of cells stained with a DNA-specific dye measured by flow cytometry. Cytometry B Clin Cytometry 1986;7:104–106.
8. Stokke T, Holte H, Smeland EB, Lie SO, Steen HB. Differential chromatin structure-dependent binding of 7-aminoactinomycin D in normal and malignant bone marrow hematopoietic cells. Cancer Res 1992; 52:5007–5012.
9. Robinson JP, Rajwa B, Gregori G, Jones J, Patsekin V. Multispectral cytometry of single bio-particles using a 32-channel. Proc SPIE-Int Soc Opt Eng 2005;5692:359–365.
10. Isailovic D, Li HW, Phillips GJ, Yeung ES. High-throughput single-cell fluorescence spectroscopy. Appl Spectrosc 2005;59:221–226.
11. Ma YF, Shortreed MR, Yeung ES. High-throughput single-molecule spectroscopy in free solution. Anal Chem 2000;72:4640–4645.
12. Wade CG, Rhyne RH, Woodruff WH, Bloch DP, Bartholomew JC, Basiji D, Ortyn WE, George TC, Brawley J, Hall BE. Characteristics and applications of imagestream(TM) multispectral imaging flow cytometry. Cytometry B Clin Cytometry 2004;59:87–92.
13. George TC, Hall BE, Zimmerman CA, Frost K, Seo M, Ortyn WE, Basiji D, Morrissey P. Distinguishing modes of cell death using imagestream(TM) multispectral imaging cytometry. Cytometry B Clin Cytometry 2004;59:118.
14. Morrissey P, George TC, Hall BE, Zimmerman CA, Frost K, Seo M, Ortyn WE, Basiji D, Philip MJ. Quantitation of nuclear translocation

events using imagestream(TM) multispectral imaging cytometry. Cytometry B Clin Cytometry 2004;59:121.
15. Brawley J, George TC, Hall BE, Frost K, Zimmerman CA, Seo M, Basiji D, Ortyn WE, Morrissey P. Fluorescent in situ hybridization in suspension analysis using imagestream(TM) multispectral imaging flow cytometry. Cytometry B Clin Cytometry 2004;59B:130.
16. Wade CG, Rhyne RH, Woodruff WH, Bloch DP, Bartholomew JC. Spectra of cells in flow cytometry using a vidicon detector. J Histochem Cytochem 1979;27:1049–1052.
17. Talmi Y. Applicability of TV-type multichannel detectors to spectroscopy. Anal Chem 1975;47:A658.
18. Warner IM, Callis JB, Davidson ER, Christian GD. Multicomponent analysis in clinical-chemistry by use of rapid scanning fluorescence spectroscopy. Clin Chem 1976;22:1483–1492.
19. Gauci MR, Vesey G, Narai J, Veal D, Williams KL, Piper JA. Observation of single-cell fluorescence spectra in laser flow cytometry. Cytometry 1996;25:388–393.
20. Robinson JP. Multispectral cytometry: The next generation. Biophotonics Int 2004;11:36–40.
21. Fuller RR, Sweedler JV. Characterizing submicron vesicles with wavelength-resolved fluorescence in flow cytometry. Cytometry B Clin Cytometry 1996;25:144–155.
22. Dubelaar GBJ, Gerritzen PL, Beeker AER, Jonker RR, Tangen K. Design and first results of CytoBuoy: A wireless flow cytometer for in situ analysis of marine and fresh waters. Cytometry B Clin Cytometry 1999;37:247–254.
23. Jett J, Albright K, Graves S, Habbersett R, Martin J, Naivar M, Parson J, Wilder M, Yoshida T. Spectral analysis flow cytometry. Cytometry Suppl 2002;11:142.
24. Franks F. Water, a Comprehensive Treatise, Vol. 1: The Physics and Physical Chemistry of Water. New York: Plenum; 1972.
25. Walker JH, Saunders RD, Hattenburg AT. NBS Measurement Services: Spectral Radiance Calibrations. Washington, DC: NBS Spectral Publications; 1987. pp 250, 251.
26. Hollberg L, Oates CW, Wilpers G, Hoyt CW, Barber ZW, Diddems SA, Oskey WH, Bergquist JC. Optical frequency/wavelength references. J Phys B: At Mol Opt Phys 2005;38:5469–5495.
27. Waymouth J. Electric Discharge Lamps. Cambridge, MA: MIT Press; 1971.
28. Maki A, Wells J. Wavenumber Calibration Tables from Heterodyne Frequency Measurements. Washington, DC: NIST Spectral Publications; 1991.
29. Layer HP, Deslattes RD, Schweitzer WG Jr. Laser wavelength comparison by high resolution interferometry. Appl Opt 1976;15:734–743.
30. Bare WD, Demas JN. Monochromator wavelength calibration standards extending into the near-infrared using second- and third-order emission lines from mercury vapor lamps. J Fluoresc 2000;10:317–324.
31. Dovichi NJ, Martin JC, Jett JH, Trkula MJ, Keller RA. Laser induced fluorescence of flowing samples as an approach to single molecule detection in liquids. Anal Chem 1984;56:348–354.
32. Cui Y, Golob J, Kelleher E, Ye ZH, Pardoll D, Cheng LZ. Targeting transgene expression to antigen-presenting cells derived from lentivirus-transduced engrafting human hematopoietic stem/progenitor cells. Blood 2002;99:399–408.
33. Huynen MA, Snel B, von Mering C, Bork P, Frishman D, Schwartz A, Wang L, Early E, Gaigalas A, Zhang YZ. Quantitating fluorescence intensity from fluorophore: The definition of MESF assignment. J Res Natl Inst Stand Technol 2002;107:83–91.
34. Gaigalas AK, Wang LL, Schwartz A, Marti GE, Vogt RF, et al. Quantitating fluorescence intensity from fluorophore: Assignment of MESF values. J Res Natl Inst Stand Technol 2005;110:101.
35. Wood JCS, Hoffman RA. Evaluating fluorescence sensitivity on flow cytometers: An overview. Cytometry B Clin Cytometry 1998;33:256–259.
36. Wood JCS. Fundamental flow cytometer properties governing sensitivity and resolution. Cytometry B Clin Cytometry 1998;33:260–266.
37. Chase ES, Hoffman RA. Resolution of dimly fluorescent particles: A practical measurement of fluorescence sensitivity. Cytometry B Clin Cytometry 1998;33:267–279.
38. Gao XH, Nie SM. Quantum dot-encoded mesoporous beads with high brightness and uniformity: Rapid readout using flow cytometry. Anal Chem 2004;76:2406–2410.
39. Wood JCS, Hamelik R. Understanding the correct usage and limitations of fluorescence spectral compensation. Cytometry B Clin Cytometry 2000;42:325.
40. Zhang YZ, Kang HC, Kemper C, Haugland RP. Stable flow cytometry calibration standards for spectral compensation. FASEB J 1996;10:458.
41. Diamond RA. Coloring up: A Guide to Spectral Compensation Springer Lab Manuals. In: Diamond RA, DeMaggio S, editors. Living Color: Protocols in Flow Cytometry and Cell Sorting. Berlin: Springer; 2002. pp 92–97.
42. Thomas O, Theraulaz F, Domeizel M, Massiani C. UV spectral deconvolution: A valuable tool for waste water quality determination. Environ Technol 1993;14:1187–1192.
43. Allyson JD, Sanderson DCW. Spectral deconvolution and operational use of stripping ratios in airborne radiometrics. J Environ Radioact 2001;53:351–363.
44. Body D, Chadwick BL. Optimization of the spectral data processing in a LIBS simultaneous elemental analysis system. Spectrochim Acta Part B 2001;56:725–734.
45. Zhang YZ, Kang HC, Kemper C, Haugland RP, Callahan MR, Rose JB, Garcia-Rubio L. Use of multiwavelength transmission spectroscopy for the characterization of *Cryptosporidium parvum* oocysts: Quantitative interpretation. Environ Sci Technol 2003;37:5254–5261.
46. Bowden R, Mitchell TA, Sarhadi M. Cluster based nonlinear principle component analysis. Electron Lett 1997;33:1858–1859.
47. Deco G, Parra L. Non-linear feature extraction by redundancy reduction in an unsupervised stochastic neural network. Neural Netw 1997;10:683–691.
48. Chibani Y, Houacine A. Redundant versus orthogonal wavelet decomposition for multisensor image fusion. Pattern Recognit 2003;36:879.
49. Duta N, Jain AK, Dubuisson-Jolly MP. Automatic construction of 2D shape models. IEEE Trans Pattern Anal Mach Intell 2001;23:433–446.
50. Tenberge JMF, Bekker PA. The isotropic scaling problem in generalized procrustes analysis. Comput Stat Data Anal 1993;16:201–210.
51. Krasnowska EK, Gratton E, Parasassi T. Prodan as a membrane surface fluorescence probe: Partitioning between water and phospholipid phases. Biophys J 1998;74:1984.
52. June CH, Rabinovitch PS. Intracellular ionized calcium. Methods Cell Biol 1994;41:149–174.
53. Nolan JP, Sklar LA. Suspension array technology: Evolution of the flat-array paradigm. Trends Biotechnol 2002;20:9–12.